INFLUENCE OF NITROGEN ENVIRONMENT ON THE PERFORMANCE OF CONDUCTING POLYMERS/CNTs NANOCOMPOSITES MODIFIED ANODES FOR MICROBIAL FUEL CELLS (MFCs)

ANCA DUMITRU[1], S. VULPE[1,2], A. RADU[1], S. ANTOHE[1,3,*]

[1]University of Bucharest, Faculty of Physics, PO Box MG-11, 077125, Magurele, Romania
[2]National Institute for Research and Development in Microtechnologies – IMT-Bucharest, 126A, Erou Iancu Nicolae Street, 077190, Bucharest, Romania
[3]Academy of Romanian Scientists, 54 Splaiul Independentei, 0505094 Bucharest, Romania
[*]*Corresponding author*: santohe@solid.fizica.unibuc.ro

Received October 30, 2017

Abstract. The development of nanocomposite materials based on conducting polymers and *carbon nanotubes* (CNT) due to their synergistic effect may offer improved performances of the devices used especially in the electrochemical applications. *Polyaniline* (PANI) and *polypyrrole* (PPY) where used to prepare the conducting polymers/CNT nanocomposites. The nature of nitrogen environment was correlated with the performances of nanocomposite modified anode for *Microbial Fuel Cells* (MFCs). The contribution of individual nitrogen type to overall surface concentration was determined using N1s high resolution *X-ray photoelectron spectroscopy* (XPS). The maximum power densities were obtained for MFCs anode modified with PANI-CNT (202.3 mW/m^2) *vs* PPY-CNT (167.8 mW/m^2) and CNT (145.2 mW/m^2).

Key words: polyaniline-CNT, polypyrrole-CNT, nanocomposite, nitrogen environment, anode modification, microbial fuel cell.

1. INTRODUCTION

Microbial fuel cell (MFC) is an emerging technology that converts the energy released by breaking chemical bonds of organic compounds, into electrical energy through catalytic reactions of microorganisms under anaerobic conditions. Even with the remarkable improvements in power density, the large-scale application of MFCs has not yet to be implemented due to low yields of power generation and high costs.

The surface characteristic of anode materials and affinity for living bacterial cells are the main factors that affect bacterial attachment, electron transfer and substrate oxidation. Most of the improvements of MFCs performance were correlated with different modification strategies of traditional carbon anode [1, 2].

Carbon nanotubes (CNT) have attracted enormous research attention in various scientific communities, due to their outstanding physicochemical properties and have shown excellent performances as anodes modifying materials in MFCs [3–7]. The impacts of CNTs types in CNT-based anodes were investigated to determine their effect on both efficiency of wastewater treatment and power generation [8]. According with other studies the introduction of functional group (O or N functionality) on the surface of CNT could be an useful method to improve bacteria attachment, electron transfer and substrate oxidation [9–11]. Some attempts have been made to synthesize conducting polymer/carbon nanotubes nanocomposite [12–14], due to their synergistic effect which may produce better applications than the individual materials, combining the redox electrochemistry of conducting polymers with high surface area and electrical conductivity of CNT [15–17].

The aim of this study is the correlation of the nature of nitrogen environment in *polypyrrole/carbon nanotubes* (PPY-CNT) and *polyaniline/carbon nanotubes* (PANI-CNT) composite materials with the performances of nanocomposite modified anode for MFCs.

2. EXPERIMENTAL DETAILS

2.1. MATERIALS

MWCNTs with diameters between 20 and 40 nm were purchased from Shenzhen Nanotech Co. Ltd. (CNT). The aniline (An) and Pyrrole (Py) monomers (Sigma Aldrich) were distilled under reduced pressure. All other chemicals including ferric chloride, *ammonium persulfate* (APS) and *methyl orange* (MO) were used without further treatment. All the solutions were prepared using deionized water.

2.2. NANOCOMPOSITE SYNHTESIS

2.2.1. Synthesis of polypyrrole/carbon nanotube nanocomposite

Polypyrrole/carbon nanotubes composites were synthesized using the modified procedure reported by Yang *et al*., where a fibrillar complex of anionic azo dye MO (*methyl orange*) and oxidant $FeCl_3$ as a reactive self-degradable seed template [18] were used. 1.5 mmol of $FeCl_3$ was dissolved in 125 ml of 5 mM MO and a flocculent precipitate appeared immediately. Then 0.5 g CNTs were added in 125 ml of solution and vigorously stirred followed by the addition of 1.5 mmol of pyrrole monomer. The mixture was stirred at room temperature for 24 h. The formed precipitate was washed with deionized water/ethanol several times until

filtrate was colorless and neutral, and finally dried under a vacuum atmosphere at 60°C for 24 h. The sample was indexed as PPY-CNT.

2.2.2. Synthesis of polyaniline/carbon nanotube nanocomposite

The synthesis of polyaniline/carbon nanotubes nanocomposites were done using the procedure reported by Huang *et al*. [19]. Polyaniline/carbon nanotubes nanocomposites were synthesized using 100 ml of mixed solution of ethanol and acetic acid containg 0.5 g CNTs with a subsequent addition of 1.82 mL aniline monomer. The reaction solution is the mixed solution of 0.4 M acetic acid and 0.4 M ethanol. 5.71 g ammonium peroxydisulfate was similarly dissolved in 100 ml of mixed solution of ethanol and acetic acid. Both solutions of aniline and oxidant were precooled at 0–5 °C for 30 min and then poured rapidly into a beaker, stirred vigorously for 30 s. The mixture was left to react for 10 h at 0°C. The product was filtered and washed with deionized water and finally dried in air for 24 h to obtain the PANI-CNT.

2.3. MATERIAL CHARACTERIZATIONS

2.3.1. X-ray photoelectron spectroscopy

XPS analysis was performed with Kratos Axis Nova instrument. The spectra were excited by the monochromatized Al Kα source (1486.6 eV). Prior to individual elemental scans a survey scan was taken for all samples in order to detect the elements present. The XPS spectra were deconvoluted with the CasaXPS software, using a weighted sum of Lorentzian and Gaussian components curves after Tougaard background subtraction.

2.3.2. X-ray diffraction

X-ray diffraction patterns of samples were recorded by X-ray diffractometer model Philips PW 3710 using CuKα radiation (λ = 1.5406 Å). Data were collected over the 2θ range of 5–50^{o}, 0.025^{o} steps and 16 s counting time per step.

2.3.3. Microbial fuel cell setup and operation

A typical two chamber MFCs was used for the investigation of PPY-CNT and PANI-CNT modified anodes. Two cylindrical shaped chambers were constructed from Plexiglas, with the diameter of 4 cm and length of 3.5 cm, separated by a Nafion 117 *Proton Exchange Membrane* (PEM). The anode and the cathode were placed on the opposite sides of a plastic (Plexiglas) cylindrical chambers. Titanium wire was used to connect the electrodes to the circuit and crocodile clips were used for attachment to a 1 kΩ resistor that completed the external circuit. Anodes were made of non-wet proofed carbon cloth. The

electrodes were modified with an aqueous suspensions of CNT, PPY-CNT, and PANI-CNT (1 mg/ml) containing 0.5% Nafion. For Pt-containing cathodes, commercial Pt catalyst (40 wt%Pt/C, Alfa Aesar) ink mixed with a chemical binder (5% Nafion solution) was sprayed over carbon cloth. The amount of nanocomposite and catalyst loading on the carbon cloth is summarized in Table 1.

Table 1

MFCs configuration and Loading of studied materials on carbon cloth

	Electrode	Anode	Loading (mg/cm^2)	Cathode	Loading (mg/cm^2)
1	MFC1	CNT	1.2	40% Pt/C	0.705
2	MFC2	PPY-CNT	0.63	40% Pt/C	1.01
3	MFC3	PANI-CNT	0.86	40% Pt/C	1.01

The anode biofilms were developed on synthetic medium containing 10% by volume of inoculums form old MFCs, phosphate buffer solution (pH 7, 0.05M), metal salts, macro solution, vitamin solution, acetate (3g/L). The catholyte consisted of phosphate buffer (pH 7, 0.05M). The anode chamber was maintained under anaerobic conditions, while the cathode chamber was purged with bubbling air.

2.3.4. MFC characterization

Cell voltages across the external resistor were recorded using a Pico Data Logger ADC-24 and personal computer. The polarization and power density curves were obtained by varying the external resistor from 0.5 MΩ to 10 Ω. The Open Cell Potential (OCP) was measured after 225 min. At each resistance, MFC ran for at least 25 minutes to ensure that a stable power output had been achieved. Current density (I) was calculated as $I = V$ (cell voltage)/R(external resistance), and power density (P) was calculated as $P = I \times V$. Both I and P were normalized to the effective projected area of the anode surface.

3. RESULTS AND DISCUSSIONS

3.1. XPS STUDIES OF NANOCOMPOSITE MATERIALS

The chemical composition from XPS data of commercial carbon nanotubes shows the presence of C1s (284.1 eV) and O1s (532.1 eV) (Table 2). In the case of modified PPY-CNT and PANI-CNT, the XPS survey spectrum (not shown here) revealed the presence of carbon, oxygen, nitrogen and sulfur (Table 2).

The chemical shift of the core electron of C1s for nanocomposite materials, the increase of the line-width of the C1s peak and a shoulder at higher binding

energy (ca 285.5 eV) are correlated with a change in the chemical bonding of nanocomposite materials, due to the introduction of nitrogen and oxygen functionality, compared to pristine CNTs [20].

Table 2

Chemical composition of the samples CNT, PPY-CNT and PANI-CNT

Sample	C1s		O1s		N1s		S2p	
	(at%)	BE (eV)	(at%)	BE (eV)	(at%)	BE (eV)	(at%)	BE (eV)
CNT	284.1	98.3	532.1	1.7	–	–	–	–
PPY-CNT	285.1	74.3	531.1	13.4	399.1	9.8	168.1	2.6
PANI-CNT	285.1	80.7	532.1	7.8	400.1	9.7	164.1	1.8

The surface nitrogen groups of PPY-CNT and PANI-CNT are identified by deconvolution of their N(1s) core level spectra. Figure 1 shows the N(1s) spectra of the PANI-CNT which were deconvoluted into four peaks corresponding to =N– (quinonoid imine nitrogen) centred ~ 397.8 eV, –NH– (benzenoid amine nitrogen) ~399.2 eV, $–NH^+$ (radical cation) ~400 eV, and $=NH^+$ (imine cation) functionalities ~ 400.9 eV (13.4 at %) [21–23].

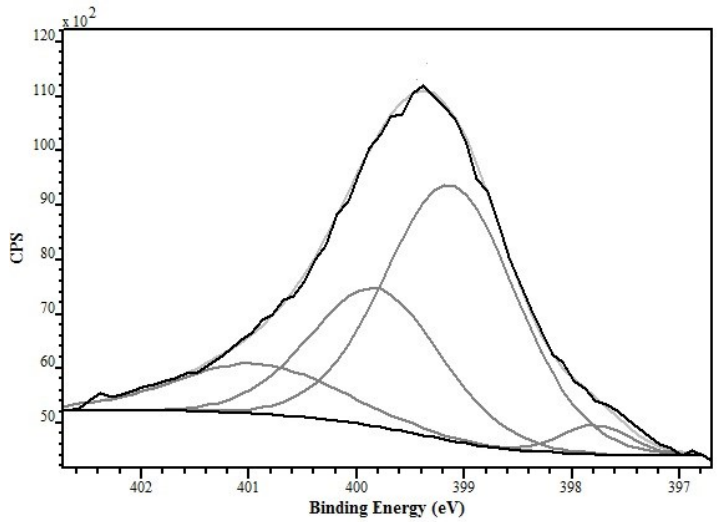

Fig. 1 – N1s core-level spectra of PANI-CNT.

Figure 2 shows the N(1s) core level spectra of the PPY-CNT which were deconvoluted into three peaks corresponding to >C=N– (neutral and imine like – structure) at ~398.1 eV, –NH– (neutral and amine-like structure) at ~399.9 eV and $–NH^+–$ (positively charged N atoms with protonation) at ~ 400.8 eV [24].

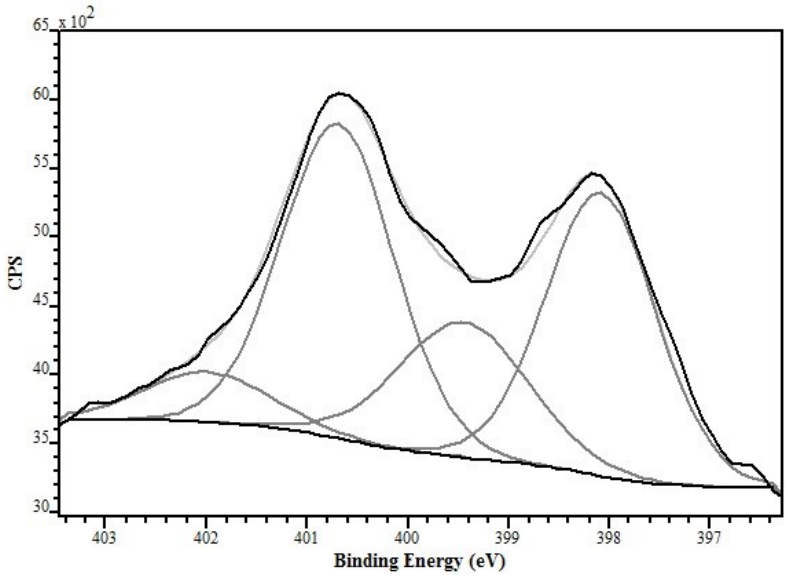

Fig. 2 – N1s core-level spectra of PPY-CNT.

Table 3

Relative quantities of surface nitrogen-containing groups of PANI-CNT and PPY-CNT

PANI-CNT					
N functionality	**=N–**	**–NH–**	**$-NH^+$**	**$=NH^+$**	**N^+/N ratio**
(at%)	3.24	54.32	29.06	13.38	0.42
PPY-CNTs					
N functionality	**imine structure >C=N–**	**neutral amine structure –NH–**		**positively charged structure $-NH^+-$**	**N^+/N ratio**
(at%)	34.69	40.75		24.52	0.24

Table 3 shows the relative quantities of surface nitrogen-containing groups and the doping level of PANI-CNT and PPY-CNT. The doping levels of the PANI-CNT were estimated by calculating the ratio of N^+ species (sum of $-NH^+$ and $=NH^+$) to N species (sum of =N–, –NH–, $-NH^+$, and $=NH^+$) [23]. The doping levels of the PPY-CNTs were estimated from the ratio of the peak area at ~401.2 eV attributed to positively charged structure to the total area of the N 1*s* peak [24, 25]. The results sumarized in Table 3 show that the dominat surface N species in both obtained materials are neutral and amine-like structures, with a higher level of doping for PANI-CNT. The higher content of positively charged nitrogen species of PANI-CNT compared with PPY-CNT, correlated with a higher

level of doping of PANI-CNT is expected to increase the charge transport properties.

3.2. X-RAY DIFFRACTION OF NANOCOMPOSITE MATERIALS

Figure 3 and Figure 4 show the X-ray diffraction patterns of PANI-CNT and PPY-CNT compared with the X-ray diffraction of PANI and PPY, obtained by similar synthesis method.

The *X-ray diffraction* (XRD) pattern of PANI shows few diffraction peaks between 10° and 30° due to the parallel and perpendicular periodicity of the polymer (PANI) chain (Fig. 3). The diffraction peak at ~ $2\theta = 6.22^{o}$ can be correlated with interplanar distance between polyaniline molecules, the broad diffraction peaks around $2\theta = 20.3^{o}$ may be ascribed to periodicity parallel to the polymer chain and the diffraction peak at $2\theta = 25.6°$ could be ascribed to periodicity perpendicular to the polymer chain [26, 27].

X-Ray diffraction patterns of nanocomposite materials show the same shape with the XRD patterns of PANI with the apparition of two supplementary peaks centred at $2\theta = 25.8^{o}$ and $2\theta = 44.1^{o}$, characteristic to (002) and (100) reflections of graphitic structure and attributed in our case to CNTs.

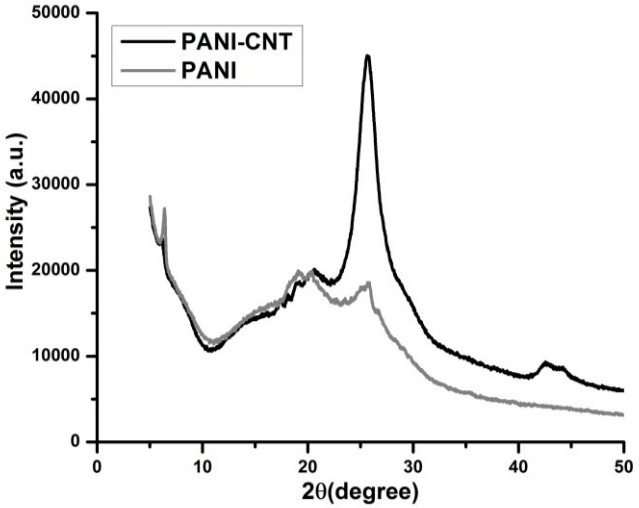

Fig. 3 – X-ray diffraction patterns of PANI and PANI-CNT.

X-ray diffraction pattern of PPY (Fig. 4) shows few diffraction peaks between 10° and 30°. The broad diffraction peak centered at ~25.6° represents the characteristic peak of amorphous polypyrrole and is due to the scattering from PPY

chains at the interplanar spacing [28, 29]. The diffraction peaks at lower angles may be attributed to the regular array of polypyrrole molecules to some extent, which produce a short of crystallinity in the polymer. The smaller peak at $2\theta = 14.28°$ can be due to the closed packing of benzene rings and indicates crystalline domains in the amorphous PPY nanowires [30]. The diffraction peaks at $2\theta = 17^o$ and $2\theta = 19^o$ represent the spacing between the ring planes of benzene ring in the adjacent PPY chains [30, 31]. The X-ray diffraction patterns of PPY-CNT have a similar shape with X-ray diffraction pattern of PPY with the addition of two supplementary peaks at 25.9^o and 42.9^o assigned to typical (002) and (100) reflections of CNTs [29].

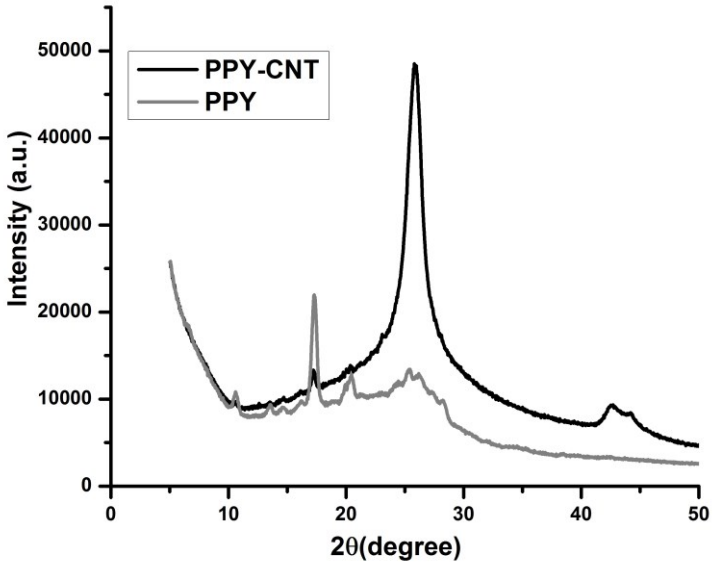

Fig. 4 – X-ray diffraction patterns of PPY and PPY-CNT.

3.3. MICROBIAL FUEL CELL PERFORMANCE

Figure 5 shows the polarization curves obtained for MFC1, MFC2 and MFC3. The OCP, maximum power density and internal resistance of the cell were summarized in Table 4.

As shown in Fig. 5, the higher *open cell potentials* (OCPs) were obtained for anode modified with nanocomposite materials (~0.8V). The maximum power densities were obtained for MFC with PANI-CNT modified carbon cloth as electrode. The potential of the cell in a batch mode and using 1 kΩ external resistor increases fast in the case of nanocomposite materials, cell potential of the MFC3 being around 550 mV just after 3 h of running.

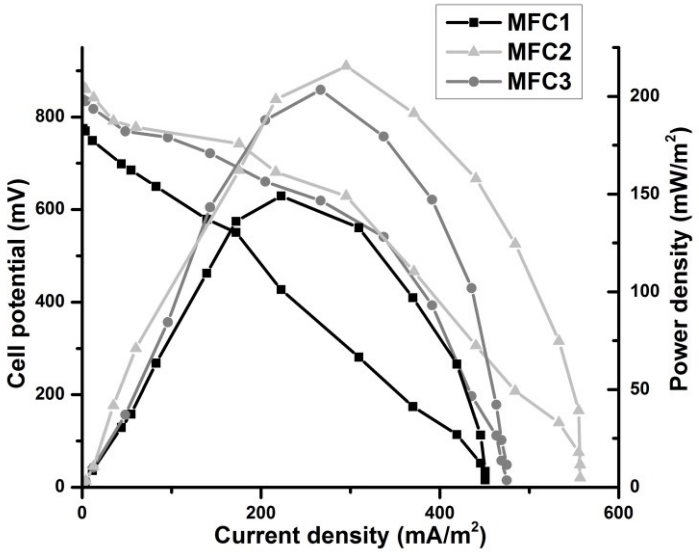

Fig. 5 – Power output and polarization curves of MFC1, MFC2 and MFC3.

Table 4

OCP, power density and internal resistance of MFC1, MFC2 and MFC3

Reactor	Anode Material	OCP (mV)	Power density (mW/m^2)	Internal resistance (kΩ)
MFC1	CNT	773	145.3	0.73
MFC2	PPY-CNT	836.5	167.8	0.64
MFC3	PANI-CNT	866.5	202.3	0.49

In the case of MFC1, the cell potential reached a value around 600 mV just after the first replacement of anolyte solution. As can be observed from Table 4, the modification of carbon cloth with nanocomposite materials give a better performance of MFCs compared with CNTs modified carbon cloth, even after a short time of running (two weeks). The maximum power density of 202.3 mW/m^2 is obtained for MFC3 with the PANI-CNT based anode. The better performance of MFCs using PANI-CNT modified anode can be correlated with the higher doping level of PANI-CNT (increase of positively charged nitrogen) which increases the charge transport properties of the nanocomposite materials.

4. CONCLUSIONS

The maximum power densities were obtained for MFCs with PANI-CNTs (202.26 mW/m^2) modified carbon cloth as electrode *vs* PPY-CNTs (167.8 mW/m^2) and CNTs (145.18 mW/m^2) modified carbon cloth. The better performance of

MFCs using PANI-CNTs modified anode was correlated with higher content of positively charged nitrogen, which increases the charge transport properties. The results regarding the conducting polymer-CNTs nanocomposite modified anode show that the conducting polymer modified anode can be an alternative for improving the MFC performances. Moreover, the results prove that the nitrogen environment of the anode surface is one important factor that can affect the perforamances of MFCs.

Acknowledgments. This work is supported by a grant of the Romanian National Authority for Scientific Research and Innovation, CNCS – UEFISCDI, project number PN-II-RU-TE-2014-4-0221.

REFERENCES

1. A. Dumitru and K. Scott, *Microbial Electrochemical and Fuel Cells. Fundamentals and Applications*, Woodhead Publishing, 117–152 (2015).
2. C. Santoro, C. Arbizzani, B. Erable, I. Ieropoulos, Journal of Power Sources **356**, 225–244 (2017).
3. H.-Y. Tsai, C.-C. Wu, C.-Y. Lec, E. P. Shih, Journal of Power Sources **194**, 199–205 (2009).
4. A. Dumitru, A. Morozan, M. Ghiurea, K. Scott, S. Vulpe, Physica Status Solidi a-Applications and Materials Science **205**, 1484–1487 (2008).
5. P. Liang, H. Wang, X. Xia, X. Huang, Y. Mo, X. Cao, M. Fan, Biosensors and Bioelectronics **26**, 3000–3004 (2011).
6. M.E. Barbinta-Patrascu, N. Badea, C. Ungureanu, C. Pirvu, V. Iftimie, S. Antohe, Romanian Reports in Physics **69**, 604 (2017).
7. Y. Zhang, L. Liu, B.V. der Bruggen, F. Yang, J. Mater. Chem. A **5**, 12673–12698 (2017).
8. N. Thepsuparungsikul, T C Ng, O. Lefebvre, H. Y. Ng, Water Science & Technology **69**, 9, 1900–1910 (2014).
9. X. Tang, K. Guo, H. Li, Z. Du, J. Tian, Bioresource Technology **102**, 3558–3560 (2011).
10. M Zhou, M. Chi, H. Wang, T. Jin, Biochemical Engineering Journal **60**, 151–155 (2012).
11. N. Zhu, X. Chen, Zhang, P. Wu, P. Li, J. Wu, Bioresource Technology **102**, 422–426 (2011).
12. Y.T. Xu, S.J. Lin, X.L. Peng, W.-A. Luo, J.-Y. Gal and L. Z. Dai, Science China Chemistry **53**, 9, 2006–2014 (2010).
13. C. L. Popa, M. Albu, C. Bartha, A. Costescu, C. Luculescu, R. Trusca, S. Antohe, Romanian Reports in Physics **68**, 1149 (2016).
14. Y. J. Zou, C. L. Xiang, L. N. Yang, L. X. Sun, F. Xu, Z. Cao, International Journal of Hydrogen Energy **33**, 4856–4862 (2008).
15. A. K. Sharma and Y.l Sharma, Journal of Electrochemical Science and Engineering **3(2)**, 47–56 (2013).
16. M. Baibarac and P. Gómez-Romero, Journal of Nanoscience and Nanotechnology **6**, 1–14 (2006).
17. R.-B. Song, Y.C. Wu, Z.-Q. Lin, J. Xie, C. H. Tan, J. S. C. Loo, B. Cao, J.-R. Zhang, J.-J. Zhu, Q. Zhang, Angewandte Chemie **129**, 10652–10656 (2017).
18. X. Yang, Z. Zhu, T. Dai, Y. Lu, Macromolecular Rapid Communication **26**, 1736 (2005).
19. Z. Huang, E. Liu, H. Shen, X. Xiang, Y. Tian, C. Xiao, Z. Mao, Materials Letters **65**, 2015–2018 (2011).
20. A. K. Chakraborty, K. S. Coleman and V. R. Dhanak, Nanotechnology **20**, 155704 (2009).
21. G. Han and S. S. Im, Polymer **41**, 3253 (2000).

22. S. M. Ahmed, European Polymer Jornal **38**, 1151 (2002).
23. S. Cho, O. S. Kwon, S. A. You and J. Jang, Journal of Materials Chemistry A **1**, 5679–5688 (2013).
24. J. Zhang, L.-B. Kong, J.-J. Cai, Y.-C. Luo, L. Kang, Electrochimica Acta **55**, 8067–8073 (2010).
25. J.H. Liu, J.W. An, Y.X. Ma, M.L. Li, R.B. Ma, M. Yu, and S.M. Li, European Physical Journal of Applied Physics **57**, 30702 (2012).
26. Z. Huang, E. Liu, H. Shen, X. Xiang, Y. Tian, C. Xiao, Z. Mao, Materials Letters **65**, 2015–2018 (2011).
27. M.A.A. El-Ghaffar, A.M. Youssef and A.A. A El-Hakim, Arabian Journal of Chemistry **8**, 6, 771–779 (2015).
28. B. Zhang, Y.g Xu, Y. Zheng, L. Dai, M. Zhang, J. Yang, Y. Chen, X. Chen and J. Zhou, *Nanoscale Research Letters* **6**, 431 (2011).
29. M. A. Chougule, S. G. Pawar, P. R. Godse, R. N. Mulik, S. Sen, V. B. Patil, Soft Nanoscience Letters, 1, 1, 6–10 (2011).
30. Z. D. Kojabad, S. A. Shojaosadati, Materials and Design, **96**, 378–384 (2016).
31. S. Bilal, F. Perveen, A.H. A. Shah, Journal of Scientific and Innovative Research **4(1)**, 33–42 (2015).